CHEMICAL ENGINEERING TRANSACTIONS
VOL. 78, 2020
A publication of AIDIC
The Italian Association of Chemical Engineering
Online at www.cetjournal.it
Guest Editors: Jeng Shiun Lim, Nor Alafiza Yunus, Jiří Jaromír Klemeš

ISBN 978-88-95608-76-1; **ISSN** 2283-9216
DOI: 10.3303/CET2078047

Fabrication of Magnetic Iron Oxide/Graphene Oxide Nanocomposites for Removal of Lead Ions from Water

Lu Thi Mong Thy[a], Pham Mai Cuong[b], Tran Hoang Tu[a], Hoang Minh Nam[b], Nguyen Huu Hieu[a], Mai Thanh Phong[b,*]

[a]VNU-HCM Key Laboratory of Chemical Engineering and Petroleum Processing (CEPP Lab)
[b]Faculty of Chemical Engineering
Ho Chi Minh City University of Technology - Vietnam National University (HCMUT - VNU)
268 Ly Thuong Kiet Street, Ward 14, District 10, Ho Chi Minh City, Vietnam
mtphong@hcmut.edu.vn

In this study, magnetic iron oxide/graphene oxide (Fe_3O_4/GO) nanocomposites were prepared by *in situ* method. It was found that the suitable ratio of Fe_3O_4/GO for lead ions (Pb^{2+}) removal was 2:1 (FGO2). The adsorption conditions of Pb^{2+} onto FGO2 were studied using response surface methodology (RSM) with Box-Behnken design. In RSM model, the interactive effects of critical variables including contact time, initial concentration, and pH on the adsorption capacity were investigated. The adsorption process followed the Langmuir isotherm model. Based on these results, FGO2 could be used as an efficient adsorbent for removal of Pb^{2+} from water.

1. Introduction

The increase of heavy metal ions concentration into the water which has caused hazardous impact on human health and ecosystems. This issue is especially serious in the case of lead pollution because of the high toxicity and the bioaccumulation ability in both human bodies and in other living organisms (Kumar et al., 2014). Even at very low concentrations, lead (II) (Pb^{2+}) ions can significantly damage the human brain, kidneys, and circulatory system, leading to serious diseases such as anemia, mental disorders, and cancers (Zhao et al., 2011). Thus, the removal of Pb^{2+} ions from water has become an urgent environmental problem. Adsorption turns out to be one of the most effective solutions due to its simple treatment process, low cost, and highly efficiency (Thy et al., 2019). In recent years, graphene-based materials *have attracted interest of researchers.* Graphene oxide (GO), as a derivatives of graphene, has oxygen-containing groups on the surface such as hydroxyl, carboxyl, carbonyl, and epoxide groups, which could be used as anchoring sites for metal ion complexation and showed good prospect in water treatment (Marina et al., 2019). However, GO can be well dispersed which causes trouble in obtaining a complete recovery (Yu et al., 2019). To overcome these disadvantages, the magnetic graphene oxide-based nanocomposites have been researched. The magnetic iron oxide/graphene oxide (Fe_3O_4/GO) *has* the unique advantages of *high* adsorption capacity, chemical stability, reusability, and easy magnetic separation to make it a potential adsorbent for removal of heavy metal ions from water (Wang et al., 2012).
The purpose of this study was to investigate the adsorption ability of Fe_3O_4/GO nanocomposites for Pb^{2+} ions. Further, response surface methodology (RSM) with Box-Behnken design (BBD) was used to study the simultaneous effects of factors on the adsorption capacity.

2. Experimental

2.1 Synthesis of Fe_3O_4/GO nanocomposites

GO was prepared from graphite powder by improved Hummers' method (Marcano et al., 2010). Fe_3O_4 nanoparticles (Fe_3O_4 NPs) were prepared by *in-situ* method. Fe_3O_4/GO nanocomposites were prepared by *in-situ* method (Thy et al., 2019). Briefly, 10 mL of $FeCl_3.6H_2O$ and $FeCl_2.4H_2O$ solution was added slowly into 50

Paper Received: 15/04/2019; Revised: 03/08/2019; Accepted: 15/11/2019
Please cite this article as: Thy L.T.M., Cuong P.M., Tu T.H., Nam H.M., Hieu N.H., Phong M.T., 2020, Fabrication of Magnetic Iron Oxide/Graphene Oxide Nanocomposites for Removal of Lead Ions from Water, Chemical Engineering Transactions, 78, 277-282 DOI:10.3303/CET2078047

mL of GO suspension (6 mg/mL). The mixture was stirred and heated to 80°C at pH 10 for 2 h. The black precipitation was separated using a magnet, followed by washing with ethanol. Finally, the nanocomposites were obtained after drying at 50 °C for 24 h. The nanocomposites with different Fe_3O_4:GO mass ratios of 2:1, 3:1, and 4:1 were marked as FGO2, FGO3, and FGO4.

The characterization of nanocomposites was investigated by X-ray diffraction (XRD), Fourier transform infrared spectroscopy (FTIR), transmission electron microscopy (TEM), Brunauer-Emmett-Teller (BET) surface area, and vibrating sample magnetometer (VSM).

2.2 Adsorption experiments

Batch experiments were carried by adding 20 mg of Fe_3O_4/GO adsorbent into 20 mL of Pb^{2+} solution at room temperature. After adsorption, Fe_3O_4/GO was separated from aqueous solution by an external magnet. The residual Pb^{2+} concentration in solution was determined by inductively coupled plasma mass spectrometry (ICP-MS 7500, Agilent, USA). RSM with Box–Behnken design was used to study the significance of independent variables and thereby determining optimal conditions for adsorption process. The regression analysis was performed to estimate the response function as a second order polynomial shown in Eq(1):

$$Y = \beta_0 + \sum_{i=1}^{3} \beta_i x_i + \sum_{i=1}^{3} \beta_{ii} x_i^2 + \sum_{i=1}^{3} \sum_{j=1}^{3} \beta_{ij} x_i x_j \quad (1)$$

where Y is the predicted response; the parameter β_o, β_i, β_{ii}, and β_{ij} are the regression coefficients for intercept, linear effect, double interaction, and quadratic effect; x_i and x_j are the independent variables (Chen et al., 2011).

Contact time (A), initial Pb^{2+} concentration (B), and pH (C) were taken as three input variables and the adsorption capacity (Y) of Fe_3O_4/GO towards Pb^{2+} was taken as the response. The range and levels of the independent variables are shown in Table 1. The statistical parameters were assessed from the analysis of variances (ANOVA) using Design Expert v.11.

Table 1: Independent variables matrix and their encoded levels

No.	Independent variables	Code	Levels		
			-1	0	+1
1	Contact time (min)	A	30	60	90
2	Initial Pb^{2+} concentration (ppm)	B	200	300	400
3	pH	C	5.1	5.9	6.7

3. Results and discussion

3.1 Characterization of Fe_3O_4/GO nanocomposites

The XRD patterns of graphite, GO, Fe_3O_4, and Fe_3O_4/GO nanocomposites are presented in Figure 1a and 1b.

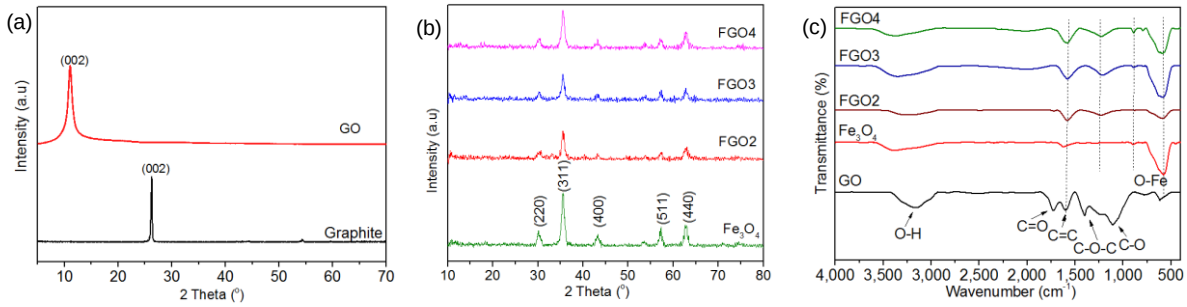

Figure 1: XRD patterns of (a) graphite and GO; (b) Fe_3O_4 NPs, and Fe_3O_4/GO nanocomposites, (c) FTIR spectra of GO, Fe_3O_4 NPs, and Fe_3O_4/GO nanocomposites

In case of GO, the diffraction peak at 2θ = 12.5° (0.8 nm) showed the formation of oxygen-containing groups on the surface of graphene sheets. In Fe_3O_4 NPs and Fe_3O_4/GO nanocomposites, several peaks at 2θ = 30.04, 35.53, 43.27, 57.31, and 62.62° were assigned to the (220), (311), (400), (511), and (440) planes (Omidinia et al., 2013). These peaks well fitted with the crystalline characteristics of Fe_3O_4 (JCPDS No.65-3107) (Chen et al., 2011). The disappearance of GO peak indicates that the Fe_3O_4 NPs were inserted between GO sheets, increasing the interlayer distance between GO sheets.

Figure 1c shows that FTIR spectrum of GO contained these peaks of oxygen-containing groups at 3,391, 1,734.5, 1,628, 1,351, and 1,098 cm^{-1}, corresponding to the stretching vibrations of hydroxyl (O-H), carbonyl

(C=O), carboxylic (COOH), epoxide (-O-), and alkoxy (C-O-C) (Shahriary and Athawale 2014, ~~2011~~). FTIR spectra of Fe_3O_4 and Fe_3O_4/GO nanocomposites showed strong fluctuations at 583 cm^{-1} corresponding toFe-O bonds in tetrahedral and octahedral sites. This result was consistent with XRD results, showed the formation of Fe_3O_4 in the structure of nanocomposites. The decrease in the intensity of oscillations at 1725 and 1599 cm^{-1} in Fe_3O_4/GO are showed that the decoration of Fe^{2+}, Fe^{3+} ions associated with high electronegativity positions on the GO surface (OH, C=O, and COOH groups), in accordance with the synthetic mechanism of the material (Kumar et al., 2014). From the above results, it can be seen that Fe_3O_4 NPs were successfully linked on GO surface.

As shown in Figure 2a, the surface of GO film was wrinkled due to the crumpling and scrolling of sheets (Metin et al., 2014). For Fe_3O_4/GO nanocomposites, the Fe_3O_4 NPs with size ranging from approximately 10-15 nm were anchored on the surface of GO sheets. The decrease in the agglomeration of Fe_3O_4 NPs showed the efficient interactions between Fe_3O_4 NPs and GO during the synthesis procedure (Trinh et al., 2018). The FGO2 had a particle size smaller, and distribution more uniform than FGO3 and FGO4. When increasing Fe_3O_4:GO ratio, the agglomeration regions and the size of Fe_3O_4 NPs were enhanced, resulting in reducing BET specific surface area as well as adsorption sites of the materials.

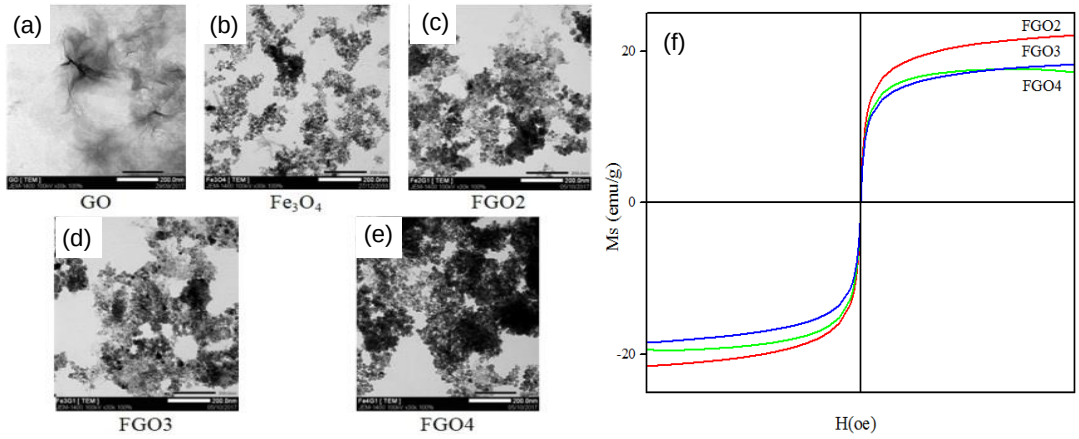

Figure 2: TEM images of (a)GO, (b) Fe_3O_4 NPs, (c) FGO2,(d) FGO3, (e) FGO4; (f) VSM data of FGO2, FGO3, and FGO4

The specific surface area of FGO nanocomposites were determined to be 190.70 - 200.40 m^2/g, which are higher than of graphene-based materials as shown in Table 2. These results could be explained by Fe_3O_4 NPs were formed and anchored on the surface of GO, decreasing the aggregation of Fe_3O_4 and stacking of GO sheets (Yang et al., 2009). However, the ratio Fe_3O_4:GO enhances, increasing the agglomeration regions of Fe_3O_4 NPs, reducing the surface area and adsorption sites (Li et al., 2013).

Table 2: BET specific surface areas of Fe_3O_4/GO nanocomposites and graphene-based materials

Materials	BET surface areas (m^2/g)	References
GO	130.20	In this study
Fe_3O_4	94.40	In this study
FGO2	200.40	In this study
FGO3	199.80	In this study
FGO4	190.70	In this study
FeOOH/GO	202.60	(Kuang et al., 2017)
$CoFe_2O_4$/Graphene	126.36	(Santhosh et al., 2015)
$NiFe_2O_4$/Graphene	57.11	(Santhosh et al., 2015)

The saturation magnetization (M_s) values of FGO2, FGO3, and FGO4 were 21.79, 18.30, and 18.54 emu/g, which were high enough to be separated by a magnet (> 16 emu/g) as shown in Figure 2f (Bai et al., 2015). These values of Fe_3O_4/GO nanocomposites were lower than that of the bulk Fe_3O_4 (92 emu/g) due to the Fe_3O_4 NPs were decorated on GO surface, decreasing in the size of nanoparticles. M_s values of Fe_3O_4/GO nanocomposites decreased from FGO2 to FGO4 due to the accumulation of Fe_3O_4 NPs, leading to an increase in particle size, reducing the magnetic value of the material (Kuang et al., 2017).

3.2 Adsorption ability of Fe_3O_4/GO nanocomposites

The Pb^{2+} adsorption capacities of FGO2, FGO3, and FGO4 were determined to be 62.35, 41.66, and 39.41 mg/g. The FGO2 has higher adsorption capacity than other ratios, which was consistent with the results of analyzing characteristic. The results of BET, TEM, and VSM showed that the FGO3 and FGO4 had the agglomeration regions of Fe_3O_4 NPs on the Fe_3O_4/GO surface, reducing the surface area and adsorption sites of materials. The increase of Fe_3O:GO ratio was also reduced the oxygen-containing groups on Fe_3O_4/GO surface, the adsorption capacities of the materials were decreased. Therefore, FGO2 was selected to study the adsorption capacity for Pb^{2+}.

3.3 Effects of adsorption variables on the adsorption capacity of FGO2

The statistical parameters from quadratic model were analysed using ANOVA to determine the suitability and reliability of the model as shown in Table 3. The F-value of model was calculated to be 48.51 indicating the model is significant. The insignificant values for of lack of fit (0.0868) and a low probability value of p-values (0.0002) were determined a very high significance for the regression model showing that the model consider to be statistically significant. The effect variables and their interactions on the responses were studied by using the comparison and evaluation with the p-values. The p-values of C_o and pH are smaller than 0.0001, thus these variables are highly significant factors. The p-values of AC, BC, and A^2 from ANOVA analysis are higher than 0.10, these coefficients are not statistically significant in model. The other variables with p-values are lower than 0.05, are significant parameters on model term. Therefore, the final equation is presented in Eq(2).

$$q = 173{,}082+1{,}404t+0{,}796C_o-99{,}892pH-0{,}00159tC_o-0{,}000833C_o^2+10{,}645pH^2 \quad (2)$$

Table 3: ANOVA analysis of the Pb^{2+} adsorption of FGO2

Source	Sum of squares	Degree of freedom	Mean square	*F*-value	*p* - value	
Model	4503.28	9	500.36	48.55	0.0002	significant
A	249.20	1	249.20	24.18	0.0044	
B	2024.71	1	2024.71	196.45	< 0.0001	
C	1647.95	1	1647.95	159.89	< 0.0001	
AB	91.49	1	91.49	8.88	0.0308	
AC	20.52	1	20.52	1.99	0.2173	
BC	1.28	1	1.28	0.1239	0.7392	
A^2	6.89	1	6.89	0.6687	0.4507	
B^2	255.97	1	255.97	24.84	0.0042	
C^2	171.30	1	171.30	16.62	0.0096	
Residual	51.53	5	10.31			
Lack of Fit	48.51	3	16.17	10.69	0.0868	not significant
Pure Error	3.03	2	1.51			
Correlation Total	4,554.81	14				

The graph of actual versus and data reveal the well-fitting with high correlation coefficients (R^2 of 0.9987 and adjusted R^2 of 0.968) suggesting a high adequacy of the models. The deviation between experimental and predicted values was low, which was inferred from the CV value (2.66 %). The difference of R^2 and the adjusted R^2 is lower than 0.2 and the value of the adequate precision is much larger than 4 (24.476), the selected model is sufficiently accurate to predict the lead ion adsorption capacity of FGO2. The individual effect of variables on the adsorption capacity for FGO2 was studied as shown in Figure 3a. The curve of B has largest slope, indicating the initial Pb^{2+} concentration had a greater effect on the adsorption capacity than time and initial concentration. This result is consistent with the higher F-value of initial Pb^{2+} concentration with respect to other process variables. Three-dimensional (3D) response surface plot has been used to study the combined effects of all the process variables on adsorption capacity of FGO2.

The adsorption capacity for the combined effect of variables at the RSM derived optimum conditions (contact time of 50 min, initial Pb^{2+} concentration of 380 ppm, and pH of 6.7) was obtained at 152.57 mg/g, which was closed to the predicted values (150.69 mg/g), indicating the suitability and accuracy of the suggested models.

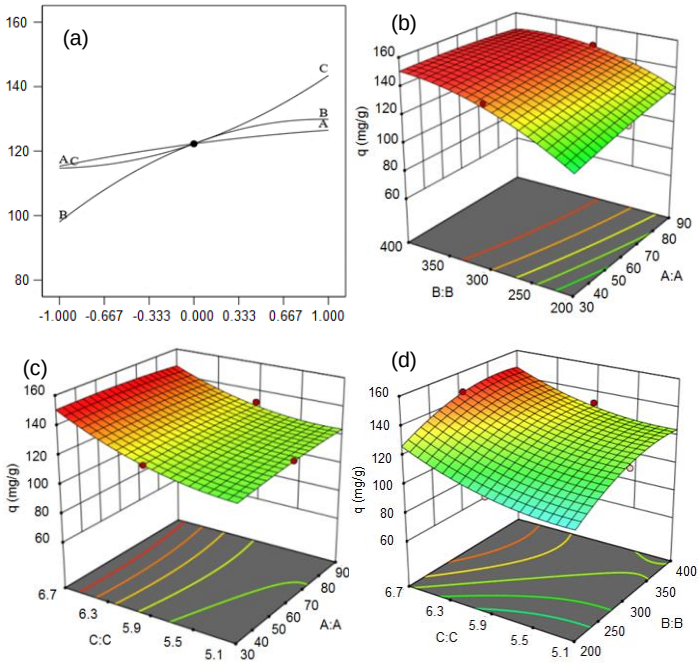

Figure 3: (a) Interaction effects of variables; 3D response surface plots for interactive effects of (b) contact time - initial Pb^{2+} concentration; (c) contact time - pH; (d) initial Pb^{2+} concentration – pHAdsorption isotherm

The adsorption data were analyzed by the Langmuir, Freundlich, and Temkin isotherm models and the results were presented in Table 4. The adsorption process was well-fitted to the Langmuir isotherm model with R^2 of 0.989 and q_{max} of 169.49 mg/g. The Langmuir isotherm is based on monolayer adsorption on the active sites of the adsorbent with constant enthalpy of adsorption for all sites.

Table 4: The parameters of Langmuir, Freundlich, and Temkin models of FGO2 for Pb^{2+} adsorption

Langmuir			Freundlich			Temkin		
k_L	q_{max} (mg/g)	R^2	n	k_F	R^2	k_T	b_T (kJ/mol)	R^2
0.027	169.49	0.989	2.94	22.65	0.934	0.43	0.08	0.953

The maximum adsorption capacities of FGO2 and other materials were presented in Table 5. FGO2 had better adsorption capacity in comparison to some other materials. The adsorption mechanism was explained by the electrostatic interaction of oxygen-containing groups on FGO2 surface with Pb^{2+}, and the formation of cation - π interactions between hexagonal structure of FGO2 with Pb^{2+} ions.

Table 5: Maximum Pb^{2+} adsorption capacities of FGO2 and other materials

Materials	q_{max} (mg/g)	References
Fe_3O_4/GO	169.49	In this study
SiO_2/Graphene	113.60	(Hao et al., 2012)
Desiccated Coconut Waste	55.86	(Abdul et al., 2019)
Kaolinite	10.40	(Tabrizi and Zamani, 2016)

4. Conclusions

Fe_3O_4/GO nanocomposites were successfully fabricated by *in-situ* method. FTIR, XRD, and TEM results showed the Fe_3O_4 NPs with size ranging from 10-15 nm were deposited on GO surface. The quadratic equations were developed to model the adsorption of Pb^{2+} based on the nanocomposite in the high experimental compatibility. The adsorption capacity of Pb^{2+} was determined at 150.69 mg/g for remaining time in 50 min with initial Pb^{2+} concentration of 380 ppm, and pH of 6.7. The obtained results proved a great potential to apply the Fe_3O_4/GO nanocomposites with the well-defined adsorption characteristics for heavy metals treatment in solution.

Acknowledgments

This research is funded by Ho Chi Minh City University of Technology, VNU-HCM, under grant number BK-SDH-2019-1880319.

References

Abdul R., Rabat N. E., Johari K., Saman N., Mat H., 2019, Removal of lead (II) ions from aqueous solution using desiccated coconut waste as low-cost adsorbent, Chemical Engineering Transactions, 72, 169-174.

Bai X., Feng R., Hua Z., Zhou L., Shi H., 2015, Adsorption of 17β-estradiol (E2) and Pb (II) on Fe_3O_4/graphene oxide (Fe_3O_4/GO) nanocomposites. Environmental Engineering Science, 32, 370-378.

Chen W., Li S., Chen C., Yan L., 2011, Self-assembly and embedding of nanoparticles by in situ reduced graphene for preparation of a 3D graphene/nanoparticle aerogel. Advanced materials, 23, 5679-5683.

Hao L., Song H., Zhang L., Wan X., Tang Y., Lv Y., 2012, SiO_2/graphene composite for highly selective adsorption of Pb (II) ion. Journal of Colloid and Interface Science, 369, 381-387.

Kuang L., Liu Y., Fu D., Zhao Y., 2017, FeOOH-graphene oxide nanocomposites for fluoride removal from water: Acetate mediated nano FeOOH growth and adsorption mechanism. Journal of Colloid and Interface Science, 490, 259-269.

Kumar P. R., Kollu P., Santhosh C., Rao K. E. V., Kim D. K., Grace A. N., 2014, Enhanced properties of porous $CoFe_2O_4$–reduced graphene oxide composites with alginate binders for Li-ion battery applications. New Journal of Chemistry, 38, 3654-3661.

Li Y., Du Q., Liu T., Sun J., Wang Y., Wu S., Xia L., 2013, Methylene blue adsorption on graphene oxide/calcium alginate composites. Carbohydrate Polymers, 95, 501-507.

Marcano D.C., Kosynkin D.V., Berlin J. M., Sinitskii A., Sun Z., Slesarev A., Tour J.M., 2010, Improved synthesis of graphene oxide. ACS Nano, 4, 4806-4814.

Marina G. B., Carmen P., Fernando G., Ángel Y., and Carmen B., 2019, CO_2 Capture by Amino-functionalized Graphene Oxide. Chemical Engineering Transactions, 75, 637-642.

Metin Ö., Aydoğan Ş., Meral K., 2014, A new route for the synthesis of graphene oxide–Fe_3O_4 (GO–Fe_3O_4) nanocomposites and their Schottky diode applications. Journal of Alloys and Compounds, 585, 681-688.

Omidinia E., Shadjou N., Hasanzadeh M., 2013, (Fe_3O_4)-graphene oxide as a novel magnetic nanomaterial for non-enzymatic determination of phenylalanine. Materials Science and Engineering: C, 33, 4624-4632.

Santhosh C., Kollu P., Felix S., Velmurugan V., Jeong S.K., Grace A.N., 2015, $CoFe_2O_4$ and $NiFe_2O_4$@ graphene adsorbents for heavy metal ions–kinetic and thermodynamic analysis. RSC Advances, 5, 28965-28972.

Shahriary L., Athawale A.A., 2014, Graphene oxide synthesized by using modified hummers approach, International Journal Renewable Energy and Environmental Engineering, 2, 58-63.

Tabrizi, N.S., Zamani S., 2016, Removal of Pb (II) from aqueous solutions by graphene oxide aerogels. Water Science and Technology, 74, 256-265.

Thy L.T.M., Thuong N.H., Tu T.H., Nam H.M., Hieu N.H., Phong M.T., 2019, Synthesis of magnetic iron oxide/graphene oxide nanocomposites for removal of cadmium ions from water. Advances in Natural Sciences: Nanoscience and Nanotechnology, 10, 025006.

Trinh L. T., Quynh L. A. B., Hieu N. H., 2018, Synthesis of zinc oxide/graphene oxide nanocomposite material for antibacterial application. International Journal of Nanotechnology, 15, 108-117.

Wang J. C., Chen P., Chen L., Wang K., Deng H., Chen F., Fu Q., 2012, Preparation and properties of poly (vinylidene fluoride) nanocomposites blended with graphene oxide coated silica hybrids. Express Polymer Letters, 6, 299-307.

Yang X., Zhang X., Ma Y., Huang Y., Wang Y., Chen Y., 2009, Superparamagnetic graphene oxide– Fe_3O_4 nanoparticles hybrid for controlled targeted drug carriers. Journal of materials chemistry, 19, 2710-2714.

Yu Y., Zhang G., Ye L., 2019, Preparation and adsorption mechanism of polyvinyl alcohol/graphene oxide-sodium alginate nanocomposite hydrogel with high Pb (II) adsorption capacity. Journal of Applied Polymer Science, 136, 47318.

Zhao G., Ren X., Gao X., Tan X., Li J., Chen C., Wang X., 2011, Removal of Pb (II) ions from aqueous solutions on few-layered graphene oxide nanosheets. Dalton Transactions, 40, 10945-10952.